Contents list available at CBIORE journal website

International Journal of Renewable Energy Development

Journal homepage: https://ijred.cbiore.id

Research Article

# Numerical evaluation of the high solidity values effect on the performance of H-Darrieus turbine with NACA 0025 hydroprofiel

José Daniel Cardona Cárdenas[a*], Juan Gonzalo Ardila Marín[a], Juan José Arbeláez Toro[b]

[a] *Department of Engineering, Universidad Surcolombiana, Neiva - Colombia*

[b] *Department of Engineering, Institución Universitaria - ITM, Medellín - Colombia*

**Abstract**. This study evaluates the performance of high-solidity H-Darrieus hydrokinetic turbines using transient two-dimensional (2D) Computational Fluid Dynamics (CFD) simulations. The objective was to analyze the impact of variations in rotor radius and blade chord length on the mechanical power generated at the shaft and on the power coefficient (Cp). Six rotors with a NACA 0025 airfoil were modeled, covering a solidity range from 1.09 to 1.64. The highest mechanical power generated was 211.6 W with a 450 mm radius rotor at a solidity of 1.09, while the maximum power coefficient (Cp,max) was 0.49. Numerical results demonstrated a strong correlation between the Cp and torque (T) as a function of the tip-speed ratio (TSR). Both magnitudes followed a similar trend, reaching their peaks within an optimal TSR range of ~2 and exhibiting analogous behavior throughout the entire performance curve. The findings confirm that for a given solidity, increasing the rotor size significantly enhances the generated torque and power. However, for the solidity values evaluated, an increase in solidity beyond 1.0 has a negative impact on the Cp. Specifically, the rotor with the highest solidity of 1.64 showed a significantly lower maximum power and Cp, in addition to a narrower operational range. The analogous behavior of the Cp trend with respect to solidity variation was corroborated by validation with the experimental findings of Dai and Lam. A discrepancy between the simulation and experimental results of between 31% and 42% was found, which is attributable to the idealizations inherent in the 2D model, such as the omission of three-dimensional effects. Despite these simplifications, the model proved to be a practical and efficient approach for the comparative analysis of turbine geometries in the initial design stages.

**Keywords:** fluid mechanics, turbomachines, hydraulic turbines, fluid dynamics, finite volume.



Received: 18th April 2025; Revised: 6th July 2025; Accepted: 10th August 2025; Available online: 26th August 2025

## 1. Introduction

Energy generation from hydrokinetic sources has emerged as a sustainable and low-impact alternative to traditional hydroelectric plants, which typically require large reservoirs and significantly alter natural water courses (Guney, 2011; Ibrahim *et al.*, 2021). H-Darrieus turbines have attracted considerable attention in this context due to their compact geometry, bidirectional operation capability, and reliable performance in low-flow river conditions (Hadad *et al.*, 2019). However, optimising their design remains a technical challenge owing to the complex fluid–structure interactions and the influence of parameters such as blade profile, number of blades, aspect ratio, and solidity—defined as the ratio between the total blade area and the rotor's swept area (Daróczy *et al.*, 2015; Horner *et al.*, 2019; Li *et al.*, 2023).

Studies on H-Darrieus turbines have employed both experimental methods and computational simulation techniques to understand their behaviour. Experimental prototypes have been developed to examine the effects of different hydrodynamic profiles and geometrical configurations (Du *et al.*, 2019; Gorle *et al.*, 2016; Padricelli, 2019; Patel *et al.*, 2017; Shimizu *et al.*, 2016; Singh *et al.*, 2015). Nonetheless, logistical constraints, high costs, and limited flexibility for systematic variations have led to widespread adoption of simulation tools, particularly Computational Fluid Dynamics (CFD), as demonstrated in the works of Benchikh *et al.* (2020), Liu *et al.* (2016), and Mohamed *et al.* (2019).

Regarding solidity, the literature indicates that most investigations focus on low values, typically below 0.9 (Mukhopadhyay *et al.*, 2024; Reddy *et al.*, 2023; Velasco *et al.*, 2017), prioritizing self-starting configurations and low starting torque requirements. Although some studies such as Dai & Lam (2009) and Sengupta *et al.* (2016) have explored higher solidity levels (>1.0), these remain rare and often lack systematic comparisons under uniform flow conditions. While more advanced approaches involving 3D simulations and fluid–structure interaction (FSI) models have been implemented (Dessoky *et al.*, 2019; Gorle *et al.*, 2021; Guevara *et al.*, 2023; Laín *et al.*, 2020), two-dimensional unsteady CFD simulations continue to be widely used due to their lower computational cost and ability to effectively capture general parametric trends.

Recently, the integration of artificial intelligence (AI) and machine learning (ML) techniques has emerged as a promising avenue to enhance the predictive accuracy of CFD simulations and to optimise key design parameters in turbomachinery. These approaches offer potential to reduce the computational cost of design iterations, improve model fidelity, and bridge gaps between numerical and experimental results. Although this study adopts a conventional CFD-based methodology, future

* Corresponding author
Email: jose.cardona@usco.edu.co (J. D. C. Cárdenas)

https://doi.org/10.61435/ijred.2025.61304
ISSN: 2252-4940/© 2025.The Author(s). Published by CBIORE

research could benefit from incorporating AI-driven optimisation and hybrid modelling techniques. Related works on AI applications in image recognition, data security, and quantum optimisation (Kh-Madhloom *et al.*, 2020; Madhloom *et al.*, 2021; Hassen *et al.*, 2025) illustrate the broad applicability and growing maturity of such methods.

Within this framework, it becomes relevant to deepen the analysis of the effects of high solidity on the performance of H-Darrieus turbines, especially when employing blade profiles such as NACA 0025, which offers geometric symmetry, structural robustness, and favourable hydrodynamic behaviour. This study addresses this gap by conducting a numerical assessment of the performance of rotors with solidity values ranging from 1.09 to 1.64, using unsteady 2D CFD simulations validated against experimental data. The aim is to evaluate how variations in rotor radius and blade chords under controlled flow conditions, influence shaft torque, power output, and the power coefficient (Cp)-key variables in the efficiency of hydrokinetic energy conversion. To achieve this aim, the study pursues the following specific objectives: (1) to geometrically model rotors of different radii and chord lengths while maintaining a controlled solidity ratio, based on configurations reported in the literature and validated through CAD tools; (2) to numerically simulate the hydrodynamic behaviour of the rotors using unsteady CFD in ANSYS Fluent, applying the k-ω SST turbulence model and the sliding mesh technique; (3) to analyse the torque, power, and Cp results as functions of the Tip Speed Ratio – TSR (Khan *et al.*, 2006), comparing trends across the various evaluated solidity configurations; and (4) to validate the numerical results against previous experimental findings (Dai & Lam, 2009) and discuss the advantages and limitations of the adopted computational approach.

## 2. Methodology

This study was carried out in five (5) stages. The first stage was the selection of the hydrodynamic profile from the results reported in the literature and in previous works (Cardona Cárdenas *et al.*, 2021; Cardona-Cárdenas *et al.*, 2023) and the two-dimensional (2D) modeling of the turbine and the determination of the boundary conditions. The second consisted of the selection of the numerical model for the fluid-dynamic solution of the phenomenon. In the third stage, the simulation parameters were configured. In the fourth stage, the discretization of the control volume was conducted, and, finally, simulations were performed by varying the TSR from 1 to 5. From this, performance curve graphs were drawn up with the results obtained. For this study, a Workstation with 48GB of RAM memory and a 2.67 GHz Intel® Xeon® processor with 12 cores in parallel with ANSYS® software (v.25.1) was utilized.

### *2.1 Turbine Modeling*

In designing the turbine rotor, the first step involved the selection of three different diameters from the work of Dai & Lam (2009). Then, the chord length was sized with respect to the rotor radius, considering the solidity ($\sigma$), defined by equation (1) as the product between the chord length (c) of the blade and the number (N) of blades of the turbine, divided by the rotor radius (R).

$$\sigma = \frac{cN}{R} \quad (1)$$

**Table 1**
Dimensions of the evaluated rotors and solidity values

| Chord (mm) | Solidity (σ) | | |
|---|---|---|---|
| | R=450 mm | R=366,8 mm | R=298,9 mm |
| 163.50 | 1.09 | | |
| 163.40 | | | 1.64 |
| 162.61 | | 1.33 | |
| 133.27 | | 1.09 | |
| 132.51 | | | 1.33 |
| 108.60 | | | 1.09 |

The solidity values and dimensions of the designed rotors are presented in Table 1. Next, the symmetrical hydrodynamic profile NACA 0025 was selected, which is one of the most studied symmetrical profiles for this type of turbine, and the number of blades was set at three. Both decisions were also based on the literature review.

To model the rotor, the coordinates of the blade geometries used for the model were exported. This was done using the online tool Airfoil Tools, where the chord length parameters and the profile reference were entered generating the files with the .cvs extension. After generating the files with the coordinates (x, y) of the points of the blade model, a data processing was performed. First, the data were separated into columns, and then a third column was added, so that three columns of data (a, x, y) were obtained.

For the third column, it was necessary to fill it with a value of one (1) until the end of the data column, when the initial value appeared again. Then the expression "polyline=true" was entered and the file was saved with a .txt extension. This procedure was performed to export the data to the SpaceClaim® module and proceed with the rotor design. This process was performed for the six rotors evaluated.

After selecting the dimensions of the turbine rotor, a 2D schematic of the complete model was developed as shown in Figure 1; it consists of two parts, a rotational domain and a stationary domain. The dimensions of the rotational domain were calculated from the rotor diameter (D), where the outer diameter is 4/3 D, and the inner diameter is 2/3 D. The moving walls of the stationary domain have a dimension of 8 D, and the fluid inlet and outlet boundaries 5 D. The rotor was located 2 ½ D from the fluid inlet. These boundaries were dimensioned with the largest D of the study (900 mm), and this was applied for the three rotor diameters selected, values reported by Lain &

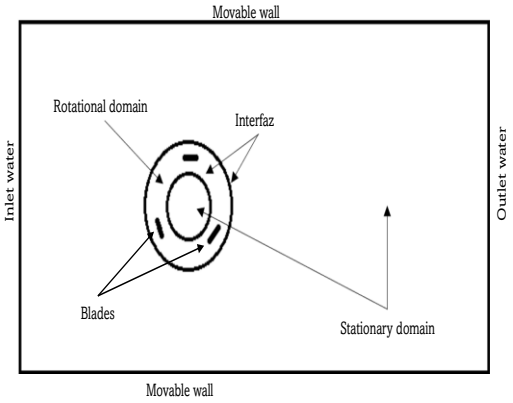


**Fig 1.** 2D model of the turbine and control volume for CFD simulation. Own source.

Osorio (Lain & Osorio, 2011). To name the boundaries, the terms presented in Figure 1 were used.

*2.2 Numerica model*

In this work, the k-ω SST (Shear Stress Transport) turbulence model, which is the most widely used in the literature (López *et al*., 2016), was implemented in the solver. It is basically a set of nonlinear equations that describe the motion of a fluid from the basic Navier-Stokes model by adding terms that explain the vortex-formation, characteristic of the turbulence. The algorithm for coupling adjustment between velocity and pressure (Semi Implicit Method for Pressure Linked Equations, or SIMPLE) was employed. This modeling approach enables the capture of turbulent pressure and shear stress gradients, facilitating the adjustment of equations for both near-wall and far-wall zone calculations, for more robust and complex solutions (ANSYS, 2025).

*2.3 Simulation parameter configuration*

Once the numerical model had been selected, the simulation parameters were configured in the ANSYS® CFD FLUENT® module. The flow solution was applied in a transient state, after which water (density ρ = 998.2 kg/m³ at 20°C) was selected as the working fluid. Subsequently, the sliding mesh model was implemented (Hashem & Mohamed, 2018; Mohamed *et al*., 2019), which simulates the physics of the rotor rotation effects. It was configured at different rotation speeds, as detailed in Table 2. The turbine rotated in a counterclockwise direction, with the flow direction entering from the left end as shown in Figure 2. The inlet flow was assigned a velocity (V) of 0.99 m/s with a turbulence percentage of 10% (López *et al*., 2016). The outlet was defined as a constant overpressure outlet of 0 Pa, and the moving walls condition of the steady state domain was applied. The residual convergence value was set to 10-3 for each time step, for a total of six complete rotor revolutions with a step time of 0.005 s for 500 iterations (González Díaz *et al*., 2016). Table 2 shows the number of steps required for the turbine to complete six full rotations (Saini & Saini, 2020). This calculation was made from equation (2) where the variable is the angular velocity (ω).

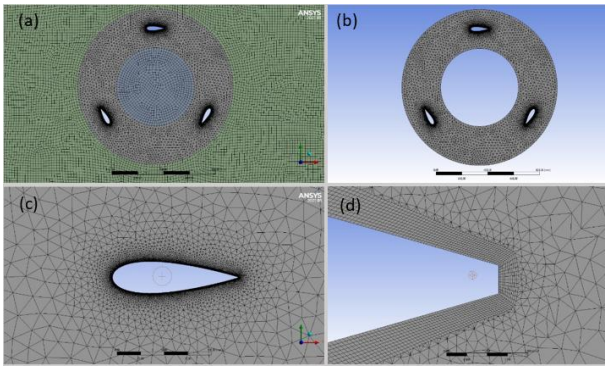


**Fig 2.** Mesh: (a) Stationary and rotational domains, (b) Detail of the rotational domain, (c) Refinement in the blade contour and (d) Detail of the inflation in the blade wall. Own source.

$$\boldsymbol{Num\ Steps} = \frac{(\boldsymbol{6\ turns})(\boldsymbol{turn})\left(\boldsymbol{\pi\ rad}/\boldsymbol{180^{\circ}}\right)}{\boldsymbol{\omega}\left[\boldsymbol{rad}/\boldsymbol{s}\right](\boldsymbol{0.005\ s})} \quad (2)$$

Table 2 shows the angular velocity calculated for the different TSR values through its definition expressed in equation (3), followed by the number of steps described above.

$$\boldsymbol{TSR} = \frac{\boldsymbol{\omega R}}{\boldsymbol{V}} \quad (3)$$

*2.4 Geometric model meshing and discretization*

Once the rotor models were developed, the meshing was carried out in the MESHING® module of ANSYS®. The general mesh size configuration was developed from cell sizes of 20 mm for the 450 mm radius rotor, 15 mm for the 366.8 mm rotor, and 10 mm for the 298.9 mm rotor. To achieve a better fit and accommodation of the elements as illustrated in Fig. 2a, an automatic square element method was employed for the stationary zone. As shown in Fig. 2b and 2c, a triangle method was used for the rotational domain to better accommodate the elements in the domain and thus improve obliquity and orthogonality. Then, a dimensioning was used on the blade faces to have a finer mesh in this area, see Fig. 2c and 2d. Next, to capture the velocity and pressure changes around the blades, an inflation of 10 layer of elements with a growth rate of 1.2 was established over the entire blade wall surface (Velasco *et al*., 2017), as illustrated in Fig. 2d. Moreover, a dimensionless wall distance, Y+ <1 (0.9), was verified and guaranteed for the blade contour, to enabling control of the viscous layer solution around the blade contour, as recommended for the implemented turbulence model (Gorle *et al*., 2021).

To guarantee the independence of the subsequent meshing outcomes, the analysis was conducted separately for each rotor configuration. The experimental setup was executed with a value of TSR = 3 to know the torque (Nm) generated by the rotor and thus determine the independence of this result with respect to the size of the mesh element. This is so because most studies find that the maximum value occurs at or near this TSR. The size variation of the element near the blade contour was carried out at three levels, resulting in a coarse mesh with minimum sizes between 0.5 and 1.0 mm, a medium classification mesh with minimum sizes between 0,03 and 0,06 mm, and a fine mesh with minimum sizes between 0,03 and 0.009 mm. In all cases the selected mesh was the median mesh,

**Table 2**
Experiment setup: own source.

| | R=0.45 m | | R=0.3668 m | | R=0.2989 m | |
|---|---|---|---|---|---|---|
| TSR ($\lambda$) | $w$ | Steps | $w$ | Steps | $w$ | Steps |
| 1 | 2.20 | 3427 | 2.70 | 2793 | 3.31 | 2278 |
| 2 | 4.40 | 1714 | 5.40 | 1396 | 6.62 | 1139 |
| 3 | 6.60 | 1142 | 8.10 | 931 | 9.94 | 759 |
| 4 | 8.80 | 857 | 10.80 | 698 | 13.25 | 569 |
| 5 | 10.10 | 747 | 13.50 | 559 | 16.56 | 455 |

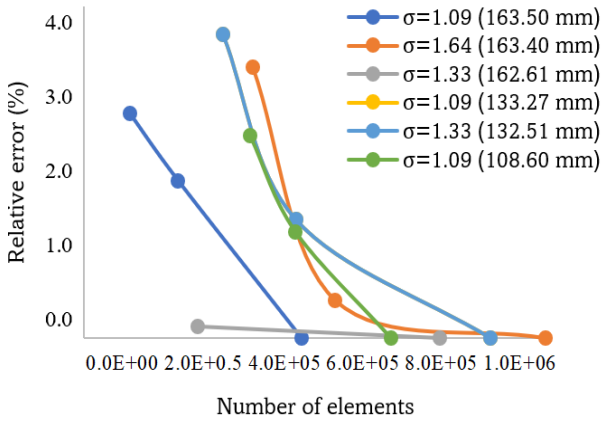


**Fig 3.** Mesh independence study. Own source.

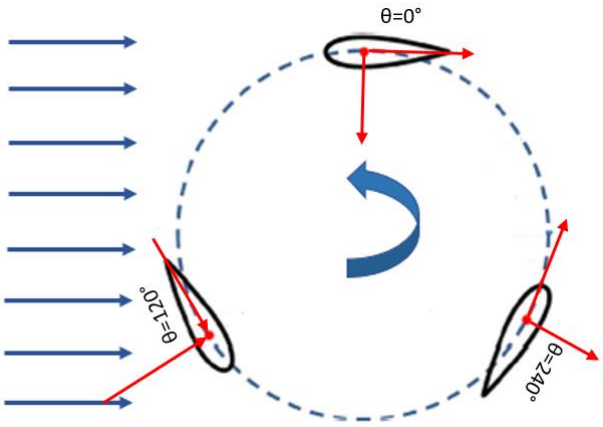


**Fig 4.** Schematic diagram of flow - turbine interaction. Own source.

which showed a relative error of less than 2.0 % in the torque with respect to the result obtained with the smallest element size. This percentage of error is admissible as reported in the literature (Benchikh Le Hocine *et al.*, 2020; Lanzafame *et al.*, 2020) and allows the computational cost to be lower (Hashem & Mohamed, 2018; Mohamed *et al.*, 2019). The median mesh that showed more elements generated 5.43E+05 elements and a relative error of 0.45 %, one of the lowest recorded, being the minimum of 0.139 %, as can be seen in Fig. 3. The median mesh that generated fewer elements reported 2.03E+05 elements and a relative error of 1.9 %, which was the highest recorded.

The operation of the H-Darrieus turbine is based on the interaction between the structure and the fluid, which produce the rotation of the rotor from the force exerted by the water on the blades. Therefore, the mechanical power (P) generated at the shaft depends on the generated torque (T) and the angular speed (ω) of the turbine rotor. Turbine performance is usually expressed in terms of the power coefficient (Cp). This power factor is defined as the ratio between the mechanical power generated in the turbine and the maximum power available in the fluid flow through the turbine. The parameters to be considered to determine this available power are the projected area of the turbine in front of the flow (A), which is determined by the rotor diameter (D) and the blade height (H) (López *et al.*, 2016), and the other parameter is the flow velocity (V). To calculate Cp, the blade height (H) was assumed to be 1000 mm and equation (4) was used.

$$C_p = \frac{P}{\frac{1}{2}\rho A V^3} = \frac{T\omega}{\frac{1}{2}\rho D H V^3} \quad (4)$$

From the simulation, the torque generated in the rotational motion of the turbine in a TSR range from 1 to 5 was obtained (Benchikh Le Hocine *et al.*, 2019; Liu *et al.*, 2016). Performance curves both for torque and power, as well as Cp, were generated for each rotor evaluated.

## 3. Results and Discussion

### *3.1 Turbine operation*

Figure 4 illustrates the operational mechanics of the turbine and the impact of water on the surface of the blades, thereby generating rotor movement. One of the advantages of this system is that the direction in which the rotor turns does not affect the operability of the turbine, but it does affect the performance in terms of power generation (Brusca *et al.*, 2015). Figure 4 describes the relationship between lift and drag forces (Gorle *et al.*, 2021). The drag force is defined as the force generated between the flow and the blade surface that is parallel to the flow direction. In contrast, the lift force is the component that is exerted perpendicular to the flow direction (Velasco *et al.*, 2017). Given the permanent change of blade position, it is understood that both forces contribute to the generation of torque at the shaft (Mohamed *et al.*, 2019). The lift and drag forces undergo a change with respect to the angle of attack during turbine rotation at varying blade positions. The tangential component of the resultant force is responsible for the generation of the torque delivered by the turbine (Abdalrahman *et al.*, 2017).

Figure 5 depicts the flow of water around the turbine, entering from the left and flowing to the right, while the turbine rotates in a counterclockwise direction. The velocity contours were obtained at the TSR at which the maximum value of Cp was observed. Due to the fixed rotational speed, recirculation occurs at varying speeds within the rotor. It is possible to observe the higher speed wake generated in the A2 blade of the rotors, which exhibits the greatest speed difference between the extrados and intrados. This is because the blade is in the position that makes the greatest contribution to the rotation of the turbine. This shows the expected behavior of the velocity contours, which illustrate the physical phenomenon of lift (Mohamed *et al.*, 2019). The three rotor blades exhibit higher

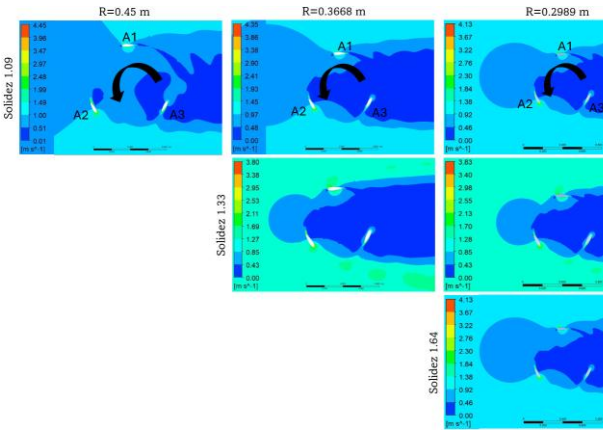


**Fig 5.** Fluid velocity contours around the rotors studied. Own source.

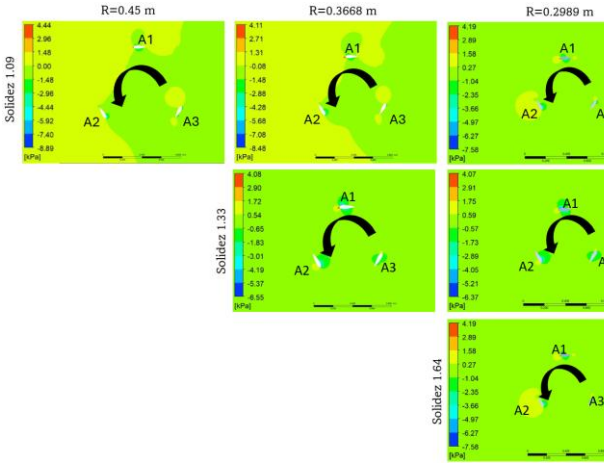


**Fig 6.** Pressure contours on the blades of the rotors studied. Own source.

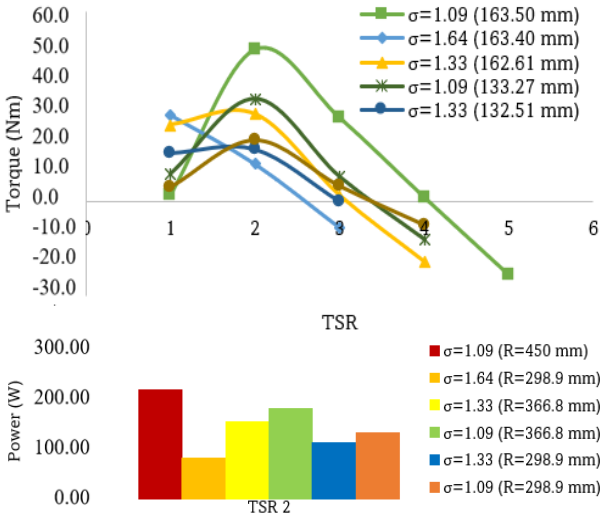


**Fig 7.** Simulation results: (a) Torque as a function of TSR, (b) Shaft power at TSR = 2. Own source.

velocities on the extrados and lower velocities on the intrados, which contributes to the generation of lift forces. Therefore, their conversion into pressure is the generator of the forces that cause rotation and torque on the shaft. It can be observed that the water wake formed downstream is less pronounced in the smallest rotor with the lowest solidity, which also has the lowest chord. This result agrees with the findings of Marsh *et al.* (Marsh *et al.*, 2015) who state that as the chord is increased while maintaining solidity, the downstream wake increases.

As illustrated in Figure 6, where the pressure contours around the rotors occur, the maximum pressure values occur at the leading edge of blade A1, though over a limited area. It is important to note that these values result in losses due to the opposition to the counterclockwise rotation of the rotor. Blade A2 experiences high pressure on the surface of the extrados, which is associated with the greatest delivery of energy from the flow to the turbine. Consequently, the relationship between the lift and the drag generated by the forces on the contours of the blades allows for greater power production (Mohamed *et al.*, 2019; Sengupta *et al.*, 2016).

Rotors with longer chord lengths, show higher pressure values. This is explained by the larger area of the profile faces (Dessoky *et al.*, 2019). In this case, both the intrados and extrados have similar areas since the NACA 0025 profile is symmetrical. This study helps to understand the phenomenon of conversion of hydraulic energy into mechanical energy. From these graphical results it is possible to observe the behavior of the contour velocity, which shows that the three blades that make up the rotor have the same behavior of wake generation at the exit or tail of the blades. Higher velocities, associated with lower pressures, occur on the faces that interact directly with the flow from left to right, generating minimum pressure compensation on the back face of the blades. This favors the lift forces to generate more power at the turbine outlet. The pressures generated at the leading edge of the A1 blade do not manage to counteract the pressure generated at the extrados of the A2 blade, without much effect on the turbine performance, thus facilitating the generation of torque on the rotor shaft.

### *3.2 Torque, power and* power coefficient

Figure 7a show the torque values achieved at each TSR and 7b the maximum power generated by the six modeled rotors at TSR = 2, the speed at which most rotors achieved their maximum torque. The rotor with the highest mechanical power was the 450 mm radius rotor with a solidity of 1.09 for a power generation of 211.60 W, followed by the 366.8 mm rotor and the same solidity with a generated power of 173.94 W. The 298.9 mm rotor with a solidity of 1.09 achieved a maximum generated power of 126.70 W, confirming the results reported in the literature, which state that for a given solidity, the rotor size should be increased to obtain a higher mechanical power generation capacity. Similarly, the rotor with a solidity value of 1.64 and a radius of 298.9 mm generated a maximum power of 77.95 W, while the rotor with the same radius but a solidity value of 1.33 generated a power of 108.42 W, suggesting that for a fixed radius and TSR, the power can be increased by decreasing the solidity in the evaluation range of the present study.

Figure 8 shows the comparative analysis between the power coefficient reached by each of the six rotors in relation to the variation of the TSR values. This is how, the characteristic behavior of the H-Darrieus type rotor can be observed, forming an inverted parabola that reaches a maximum value and then begins to decrease (Liu *et al.*, 2016). Figure 8 shows that five of the six rotors reach their maximum value of Cp when TSR = 2, as in Dessoky *et al.* (Dessoky *et al.*, 2019). However, the rotor with higher solidity shows an atypical behavior and reaches a maximum Cp at TSR = 1 as in Kumar *et al.* (Kumar *et al.*, 2017) and starts to decrease until reaching negative values at TSR = 3. The maximum Cp value obtained in this numerical study was obtained with the rotor having a radius of 450 mm and a chord of 163.50 mm, i.e. the one with solidity of 1.09, giving a maximum Cp value of 0,49, matched by the 366.8 radius rotor with 133.27 mm chord, solidity of 1.09 again. The lowest maximum Cp value of the study was 0,31 for the 298.9 rotor whose chord was 163.40 mm, i.e. the one with highest solidity, of 1.64. This again suggests that increasing solidity in this high rating range has a negative effect on Cp.

Furthermore, Figure 8 also shows that the larger rotor has a wider TSR operating range than the rest of the implemented rotors, which turns out to agree with what was said by Çetin *et al.* (Çetin *et al.*, 2005). The negative values of torque and Cp outside the operating range of each rotor correspond to speeds so high that, if present, they would experience a braking effect or counter-torque by the flow. A comparison of these results with others in the literature reviewed, it was found that the maximum Cp achieved by the rotor configured with radius 450

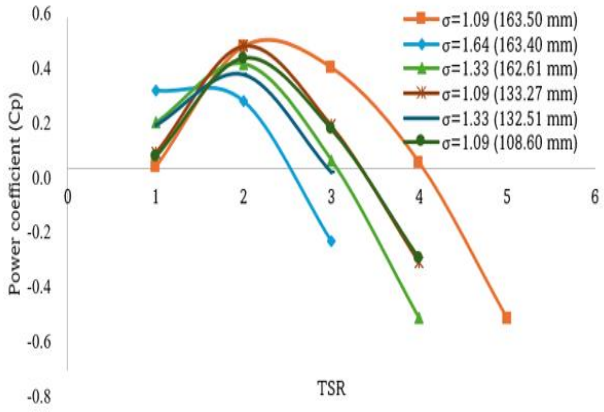


**Fig 8.** Simulation results: Power coefficient as a function of TSR. Own source.

mm and solidity 1.09 reached a value of 0.49 for TSR = 2, a higher result than that reported in the numerical study by López *et al.* (2016), which was 0.35 for a TSR = 1.65 with the same radius and profile.

Based on the obtained data, a strong correlation is observed between the power coefficient (Cp) and the torque (T) as a function of the tip-speed ratio (TSR). Both magnitudes exhibit a similar trend, increasing as the TSR rises from 1, reaching a maximum value within an optimal TSR range around 2, and subsequently following the same descending trend. Specifically, the points of maximum power coefficient align closely with the points of maximum torque for each rotor configuration. This behavior reflects that the maximum aerodynamic efficiency, as measured by Cp, is achieved precisely when the rotor generates its maximum torsional moment. Beyond these peaks, the correlation is maintained throughout the entire curve, as the general behavior of Cp replicates that of the torque: any increase or decrease in torque directly translates into an analogous change in the power coefficient, thus demonstrating that the rotor's capacity to extract energy from the wind is intrinsically linked to its ability to generate torque. Furthermore, it is evident that configurations generating a higher shaft torque exhibit a broader operational range before reaching the negative torque limit, which occurs when the angular velocity is so high that the airflow tends to brake the rotor rather than drive it.

Figure 9 compares the numerical results achieved against the results achieved experimentally by Dai & Lam (Dai & Lam, 2009). The behavior is similar and validates the notion that an increase in solidity has a negative impact on turbine performance for this high range of values, and it shows that to improve the efficiency of an H-Darrieus turbine, under these constructional characteristics with an established robustness value, a larger rotor diameter is required. As anticipated, the results of the CFD model implemented in this work exceed those reported by the experimental study. While the percentage differences are between 31 and 41% respectively, it should be noted that the numerical results do not exceed the limit set by Betz. (Guney, 2011). Besides, the 2D numerical model has disadvantages, such as the implementation of constant velocities over the entire projected area of the turbine over the flow (Liu *et al*., 2016) compared to the experimental work, where the references generate conditions of natural turbine rotation, realistic situations that are not idealized. Therefore, the computational fluid dynamics (CFD) model does not present the limitations of variable flow velocity, friction due to particles in the fluid, and other conditions imposed by the experimental environment that the solver does not estimate to perform the calculations. Even so, these numerical results allow knowing the behavior of the H-Darrieus type rotor under some established conditions to predict its operation under natural conditions.

While the numerical results obtained in this study exhibited the expected trend and were generally consistent with the experimental findings of Dai & Lam (2009), it is important to consider the computational efficiency and specificity of the implemented CFD model. These aspects are particularly relevant when comparing the present methodology with more complex or alternative numerical techniques. The transient two-dimensional (2D) simulations were performed using ANSYS Fluent on a workstation equipped with a 12-core Intel® Xeon® processor (2.67 GHz) and 48 GB of RAM. The median mesh for the largest rotor configuration consisted of approximately 543,000 elements. For each TSR value simulated, six complete revolutions of the rotor were computed using a time step of 0.005 s and a convergence criterion of $1\times10^{-3}$. Under these settings, each simulation required approximately 6–8 hours of computational time. Compared to three-dimensional (3D) simulations or hybrid turbulence models such as LES or DES, the 2D k-ω SST model employed here provided a substantially lower computational cost. This trade-off allowed for the exploration of multiple rotor configurations within a reasonable timeframe, making the model suitable for parametric design studies where geometric variables such as solidity and chord length must be varied systematically.

The model used in this study was specifically configured for H-Darrieus turbines operating in uniform, subcritical hydrokinetic flows at low velocities (~0.99 m/s), with symmetrical NACA 0025 profiles and fixed rotational domains. This configuration effectively captures the dominant hydrodynamic effects and enables the calculation of torque and power coefficients across a range of TSR values. However, several limitations are inherent to the modelling approach: (1) The 2D framework does not account for end effects, three-dimensional wake structures, or spanwise flow, which may influence the accuracy of results in practical scenarios. (2) Wall roughness, turbulence anisotropy, and unsteady blade–vortex interactions are simplified or excluded. (3) The model assumes rigid, non-deformable blades, and thus does not capture any fluid–structure interaction (FSI) effects. Despite these simplifications, the model exhibited consistent trends with experimental results and fulfilled the objective of analysing the influence of high solidity values on turbine performance. For design optimisation tasks where fast iteration and geometric sensitivity are priorities, the present approach strikes a balance between computational practicality and physical relevance. Future work could incorporate AI-based surrogate models or multi-objective optimisation techniques to complement CFD simulations, reduce error margins, and further refine turbine design.

## 4. Conclusion

The variation of the rotor radius and the chord length, using solidities of 1.09; 1.33 and 1.64; were evaluated for a total of six rotor models with the hydrodynamic profile NACA 0025, studying their incidence on the mechanical power generation at the shaft and on the performance of H-Darrieus turbines. The CFD model in transient state used to simulate the rotor behavior predicted a parabolic behavior of Cp under the configuration of different TSR values from 1 to 5, with maximum values at TSR 2. The numerical results obtained were contrasted with the

experimental results reported by Dai & Lam, (2009), which show the same behavior, i.e. a negative effect on the performance as the solidity increased beyond the 1.0 threshold.

Moreover, the modeling process yielded results for torque, power, and power coefficient generated by the rotors, determining the maximum and minimum conditions of each rotor for evaluated TSR values. This is how the rotor whose geometric characteristics of 450 mm radius and chord length of 163.50 mm, reached a maximum generated torque of 48.09 Nm and a power of 211.60 W, which is 49.25% higher than that of the rotor with 366.8 mm radius for the same solidity value of 1.09. Therefore, it is confirmed that the rotor diameter should be increased to improve performance and power generation for a given solidity value.

Therefore, the 450  and 366.8 mm radius rotors show a wider operating range in relation to the variation of the TSR values, which range from 1 to 4 until reaching the braking zone. On the other hand, the rotor with a radius of 298.9 mm and a solidity of 1,64 has a much smaller operating range, since it is between TSR values 1 and 3, reaching its maximum torque and Cp value at TSR = 1. This makes it necessary to evaluate this rotor under conditions of TSR values below 1.

From the velocity and pressure contour figures, the impact of changes in solidity and chord for each evaluated rotor radius was observed. This confirmed the physical phenomenon of velocity difference between the extrados and intrados of the hydrodynamic profiles and how the lower velocities are associated with the higher pressures, which cause the lift and drag forces that generate the rotation and torque in the rotor due to the interaction of the fluid and the turbomachine.

The results of this study, which were compared with the experimental studies of Dai & Lam, (2009), showed a similar behavior with respect to the trend of the power coefficient versus the solidity value for the six rotors. This is how the difference between the simulation results and the experimental results achieved by the benchmark was 41%, 41% and 34% for the rotors with a solidity of 1,09. As well, for the solidity of 1.33; the difference between the numerical and experimental results was 38% and 31%, respectively. And finally, the difference between the numerical and experimental results for the solidity rotor of 1.64 was 32%. It should be noted that both the experimental and numerical studies have some limitations, which means that the results can vary significantly.

In addition to the performance-related findings, the study demonstrated that the adopted two-dimensional transient CFD model offers a practical balance between computational efficiency and predictive capability. Although the model introduces simplifications that limit the capture of certain three-dimensional effects, it remains well-suited for comparative analysis of turbine geometries, particularly in early-stage design iterations. The relatively low computational cost enabled a systematic evaluation of high solidity values, contributing valuable insights into their impact on H-Darrieus turbine performance. Future research may benefit from integrating AI-based optimisation frameworks or higher-fidelity simulations to enhance accuracy and broaden applicability.

Further research is encouraged to enhance the physical fidelity of the model by incorporating three-dimensional CFD simulations, particularly to capture spanwise flow effects and blade tip vortices. Additionally, experimental validation under variable flow conditions would strengthen the reliability of numerical predictions. The integration of artificial intelligence (AI) and machine learning (ML) tools could also support the development of surrogate models and optimisation frameworks, enabling faster and more cost-effective design iterations. Finally, extending the analysis to include unsteady inflow conditions, structural flexibility, and different blade profiles would broaden the applicability of the findings and contribute to more robust hydrokinetic turbine designs.

## Acknowledgments

The authors express their gratitude to the Universidad Surcolombiana, especially to ITM and its simulation, modeling, and prototyping laboratory, for their support with hardware, software (ANSYS V25.1 Engineering Software Licensing), and connectivity, which were central factors in the proposed project.

**Author Contributions**: Conception and design of the analysis, as well as data collection: J. Cardona. Contribution of data and analysis tools: J. Cardona and J. Ardila. Conducting the analysis and writing the article: J. Cardona, J. Ardila, and J. Arbeláez.

**Funding:** The project was sponsored by the Institución Universitaria - ITM, which provided software, hardware and human talent, and the Universidad Surcolombiana, which provided human talent.

**Conflicts of Interest:** The authors certify that they have no conflicts of interest pertaining to this research, whether financial, personal, authorship-related, or otherwise, that could potentially influence the research, or the results presented in this document.

## References

Abdalrahman, G., Melek, W., & Lien, F. S. (2017). Pitch angle control for a small-scale Darrieus vertical axis wind turbine with straight blades (H-Type VAWT). *Renewable Energy*, 114, 1353–1362. https://doi.org/10.1016/j.renene.2017.07.068

ANSYS. (2021). Ansys Fluent Theory Guide.

Benchikh Le Hocine, A. E., Jay Lacey, R. W., & Poncet, S. (2019). Multiphase modeling of the free surface flow through a Darrieus horizontal axis shallow-water turbine. *Renewable Energy*, 143, 1890–1901. https://doi.org/10.1016/j.renene.2019.06.010

Benchikh Le Hocine, A. E., Poncet, S., & Lacey, J. (2020). Numerical Modeling of a Darrieus Horizontal Axis Shallow-Water Turbine. *Journal of Energy Engineering,* 146(5). https://doi.org/10.1061/(asce)ey.1943-7897.0000700

Brusca, S., Cucinotta, F., Galvagno, A., Lanzafame, R., Mauro, S., & Messina, M. (2015). Oscillating Water Column Wave Energy Converter by means of straight-bladed Darrieus turbine. *Energy Procedia,* 82, 766–773. https://doi.org/10.1016/j.egypro.2015.11.809

Cardona Cárdenas, J. D., Ardila Marín, J. G., Gutiérrez Flórez, J. M., & Vanegas, C. A. R. (2021). Vertical axis Darrieus turbines: State of the art research. *International Journal of Engineering Research and Technology,* 14(7). http://www.irphouse.com708

Cardona-Cárdenas, J. D., Zuluaga, D. A. H., Marín, J. G. A., Faria, R. de O., & Vanegas, C. A. R. (2023). Impact of Blade and Solidity on the Performance of H-Darrieus Hydrokinetic Turbines by CFD Simulation. *Revista de Gestão Social e Ambiental,* 18(1), e03224. https://doi.org/10.24857/rgsa.v18n1-007

Çetin, N. S., Yurdusev, M. A., Ata, R., & Özdamar, A. (2005). Assessment of optimum tip speed ratio of wind turbines. *Mathematical and Computational Applications,* 10(1), 147–154. https://doi.org/10.3390/mca10010147

Dai, Y. M., & Lam, W. H. (2009). Numerical study of straight-bladed Darrieus-type tidal turbine. *Proceedings of Institution of Civil Engineers: Energy,* 162(2), 67–76. https://doi.org/10.1680/ener.2009.162.2.67

Daróczy, L., Janiga, G., Petrasch, K., Webner, M., & Thévenin, D. (2015). Comparative analysis of turbulence models for the aerodynamic simulation of H-Darrieus rotors. *Energy,* 90, 680–690. https://doi.org/10.1016/j.energy.2015.07.102

Dessoky, A., Bangga, G., Lutz, T., & Krämer, E. (2019). Aerodynamic and aeroacoustic performance assessment of H-rotor darrieus VAWT equipped with wind-lens technology. *Energy,* 175, 76–97. https://doi.org/10.1016/j.energy.2019.03.066

Du, L., Ingram, G., & Dominy, R. G. (2019). Experimental study of the effects of turbine solidity, blade profile, pitch angle, surface roughness, and aspect ratio on the H-Darrieus wind turbine self-starting and overall performance. *Energy Science and Engineering,* 7(6), 2421–2436. https://doi.org/10.1002/ese3.430

Gorle, J. M. R., Chatellier, L., Pons, F., & Ba, M. (2021). Sensitivity analysis of the performance of a Darrieus hydrokinetic turbine in uncertain operating conditions. *Sustainable Energy Technologies and Assessments,* 46. https://doi.org/10.1016/j.seta.2021.101247

Guevara-Munoz, A., Hincapie-Zuluaga, D., Rio, J. S. Del, Rodriguez-Cabal, M. A., & Torres-Lopez, E. (2023). Numerical Comparison and Efficiency Analysis of Three Vertical Axis Turbine of H-Darrieus Type. *EUREKA, Physics and Engineering*, 2023(2), 28–39. https://doi.org/10.21303/2461-4262.2023.002593

Guney, M. S. (2011). Evaluation and measures to increase performance coefficient of hydrokinetic turbines. *Renewable and Sustainable Energy Reviews*,15(8), 3669–3675. https://doi.org/10.1016/j.rser.2011.07.009

Hadad, Y., Ramakrishnan, B., Pejman, R., Rangarajan, S., Chiarot, P. R., Pattamatta, A., & Sammakia, B. (2019). Three-objective shape optimization and parametric study of a micro-channel heat sink with discrete non-uniform heat flux boundary conditions. *Applied Thermal Engineering,* 150, 720–737. https://doi.org/10.1016/j.applthermaleng.2018.12.128

Hashem, I., & Mohamed, M. H. (2018). Aerodynamic performance enhancements of H-rotor Darrieus wind turbine. *Energy,* 142, 531–545. https://doi.org/10.1016/j.energy.2017.10.036

Hassen, O. A., Majeed, H. L., Hussein, M. A., Darwish, S. M., & AlBoridi, O. (2025). Quantum Machine - Learning for Video Compression: An Optimal Video Frames Compression Model using Qutrits Quantum Genetic Algorithm for Video multicast over the Internet. *Journal of Cybersecurity and Information Management*, 15(2), 43-64.

Hoerner, S., Abbaszadeh, S., Maître, T., Cleynen, O., & Thévenin, D. (2019). Characteristics of the fluid–structure interaction within Darrieus water turbines with highly flexible blades. *Journal of Fluids and Structures,* 88, 13–30. https://doi.org/10.1016/j.jfluidstructs.2019.04.011

Ibrahim, W. I., Mohamed, M. R., Ismail, R. M. T. R., Leung, P. K., Xing, W. W., & Shah, A. A. (2021). Hydrokinetic energy harnessing technologies: A review. *Energy Reports*, 7, 2021–2042). Elsevier Ltd. https://doi.org/10.1016/j.egyr.2021.04.003

González Díaz, A. J., Geovo Coronado, L. J., & González Doria, Y. E. (2016). Diseño y modelamiento de un aerogenerador Vawt Darrieus tipo H para la zona costera del departamento de Córdoba. *Ingeniare*, 20, 33–46. https://doi.org/10.18041/1909-2458/ingeniare.20.407

Gorle, J. M. R., Chatellier, L., Pons, F., & Ba, M. (2016). Flow and performance analysis of H-Darrieus hydroturbine in a confined flow: A computational and experimental study. *Journal of Fluids and Structures,* 66, 382–402. https://doi.org/10.1016/j.jfluidstructs.2016.08.003

Kh-Madhloom, J., Diwan, S. A., & Zainab, A. A. (2020). Smile Detection using Convolutional Neural Network and Fuzzy Logic. *J. Inf. Sci. Eng.*, 36(2), 269-278. https://doi.org/10.6688/JISE.202003_36(2).0007

Khan, M. J., Iqbal, M. T., & Quaicoe, J. E. (2006). Design Considerations of a Straight Bladed Darrieus Rotor for River Current Turbines. *2006 IEEE International Symposium on Industrial Electronics*, Montreal, QC, Canada, 2006, pp. 1750-1755, https://doi.org/10.1109/ISIE.2006.295835

Kumar, P. M., Ajit, K. R., Surya, M. R., Srikanth, N., & Lim, T.-C. (2017). On the self starting of Darrieus turbine :An Experimental investigation with secondary rotor. *2017 Asian Conference on Energy, Power and Transportation Electrification (ACEPT)*, Singapore, 2017, pp. 1-7, https://doi.org/10.1109/ACEPT.2017.816854

Lain, S., & Osorio, C. (2011). Simulation and evaluation of a straight-bladed Darrieus-type cross flow marine turbine. In Article in *Journal of Scientific & Industrial Research*, 69. https://www.researchgate.net/publication/229050514

Laín, S., Cortés, P., & López, O. D. (2020). Numerical simulation of the flow around a straight blade Darrieus water turbine. *Energies,* 13(5). https://doi.org/10.3390/en13051137

Li, G., Wu, G., Tan, L., & Fan, H. (2023). A Review: Design and Optimization Approaches of the Darrieus Water Turbine. *Sustainability (Switzerland),* 15(14). https://doi.org/10.3390/su151411308

Liu, Z., Qu, H., & Shi, H. (2016). Numerical study on self-starting performance of Darrieus vertical axis turbine for tidal stream energy conversion. *Energies,* 9(10). https://doi.org/10.3390/en9100789

López, O., Meneses, D., Quintero, B., & Laín, S. (2016). Computational study of transient flow around Darrieus type cross flow water turbines. *Journal of Renewable and Sustainable Energy*, 8(1). https://doi.org/10.1063/1.4940023

Madhloom, J. K., Abd Ghani, M. K., & Baharon, M. R. (2021). Enhancement to the patient's health care image encryption system, using several layers of DNA computing and AES (MLAESDNA). *Periodicals of Engineering and Natural Sciences,* 9(4), 928-947. https://doi.org/10.21533/pen.v9i4.2448

Marsh, P., Ranmuthugala, D., Penesis, I., & Thomas, G. (2015). Three-dimensional numerical simulations of straight-bladed vertical axis tidal turbines investigating power output, torque ripple and mounting forces. *Renewable Energy*, 83, 67–77. https://doi.org/10.1016/j.renene.2015.04.014

Lanzafame, R., Mauro, S., Messina, M., & Brusca, S. (2020). Micro H-Darrieus wind turbines: CFD modeling and experimental validation. *Energies,* 13, 1–23. https://doi.org/10.1063/1.5138842

Mohamed, M. H., Dessoky, A., & Alqurashi, F. (2019). Blade shape effect on the behavior of the H-rotor Darrieus wind turbine: Performance investigation and force analysis. *Energy,* 179, 1217–1234. https://doi.org/10.1016/j.energy.2019.05.069

Mukhopadhyay, A., Sharma, A., Hossain, A., Roy, S., Singha, S., Modak, D., Gupta, A. K., Shaw, A., Sarkar, A., Paul, N., Sengupta, A. R., & Rakshit, S. (2024). A Review on the Effect of Different Performance Parameters of H-Darrieus Turbines. In G. Choubey, S. Tripathi, V. K. Singh, & P. M. V Subbarao (Eds.), Advances in Thermal Engineering (pp. 195–204). Springer Nature Singapore. https://doi.org/10.1007/978-981-97-4500-5_14

Padricelli, C. (2019). CFD Investigation of counter rotating H-type Darrieus turbines in marine environment [Politecnico di Milano]. http://hdl.handle.net/10589/87083%0A%0A

Patel, V., Eldho, T. I., & Prabhu, S. V. (2017). Experimental investigations on Darrieus straight blade turbine for tidal current application and parametric optimization for hydro farm arrangement. *International Journal of Marine Energy*, 17, 110–135. https://doi.org/10.1016/j.ijome.2017.01.007

Reddy, K. U., Deb, B., & Roy, B. (2023). Experimental investigation of solidity and blade profile effects on H-Darrieus wind rotor: Performance and self-starting analysis. *Journal of Renewable and Sustainable Energy,* 15(4), 43306. https://doi.org/10.1063/5.0159494

Saini, G., & Saini, R. P. (2020). Comparative investigations for performance and self-starting characteristics of hybrid and single Darrieus hydrokinetic turbine. *Energy Reports*, 6, 96–100. https://doi.org/10.1016/j.egyr.2019.11.047

Sengupta, A. R., Biswas, A., & Gupta, R. (2016). Studies of some high solidity symmetrical and unsymmetrical blade H-Darrieus rotors with respect to starting characteristics, dynamic performances and flow physics in low wind streams. *Renewable Energy*, 93, 536–547. https://doi.org/10.1016/j.renene.2016.03.029

Shimizu, S., Fujii, M., Sasa, K., Koga, E., & Motogi, H. (2016). Starting system for Darrieus water turbine of tidal stream electricity generation. *Proceedings of the ASME 2016 35th International Conference on Ocean, Offshore and Arctic Engineering*. *Volume 6: Ocean Space Utilization; Ocean Renewable Energy*. Busan, South Korea. June 19–24, 2016. V006T09A010. ASME. https://doi.org/10.1115/OMAE2016-55143

Singh, M. A., Biswas, A., & Misra, R. D. (2015). Investigation of self-starting and high rotor solidity on the performance of a three

S1210 blade H-type Darrieus rotor. *Renewable Energy*, 76, 381–387. https://doi.org/10.1016/j.renene.2014.11.027

Velasco, D., López Mejia, O., & Laín, S. (2017). Numerical simulations of active flow control with synthetic jets in a Darrieus turbine. *Renewable Energy*, 113, 129–140. https://doi.org/10.1016/j.renene.2017.05.075